NANO LETTERS

Letter

pubs.acs.org/NanoLett

Tuning the Light Emission from GaAs Nanowires over 290 meV with Uniaxial Strain

Giorgio Signorello,* Siegfried Karg, Mikael T. Björk,† Bernd Gotsmann, and Heike Riel

IBM Research − Zurich, Säumerstrasse 4, 8803 Rüschlikon, Switzerland

Supporting Information

ABSTRACT: Strain engineering has been used to increase the charge carrier mobility of complementary metal−oxide−semiconductor transistors as well as to boost and tune the performance of optoelectronic devices, enabling wavelength tuning, polarization selectivity and suppression of temperature drifts. Semiconducting nanowires benefit from enhanced mechanical properties, such as increased yield strength, that turn out to be beneficial to amplify strain effects. Here we use photoluminescence (PL) to study the effect of uniaxial stress on the electronic properties of GaAs/$Al_{0.3}Ga_{0.7}As$/GaAs core/shell nanowires. Both compressive and tensile mechanical stress were applied continuously and reversibly to the nanowire, resulting in a remarkable decrease of the bandgap of up to 296 meV at 3.5% of strain. Raman spectra were measured and analyzed to determine the axial strain in the nanowire and the Poisson ratio in the ⟨111⟩ direction. In both PL and Raman spectra, we observe fingerprints of symmetry breaking due to anisotropic deformation of the nanowire. The shifts observed in the PL and Raman spectra are well described by bulk deformation potentials for band structure and phonon energies. The fact that exceptionally high elastic strain can be applied to semiconducting nanowires makes them ideally suited for novel device applications that require a tuning of the band structure over a broad range.

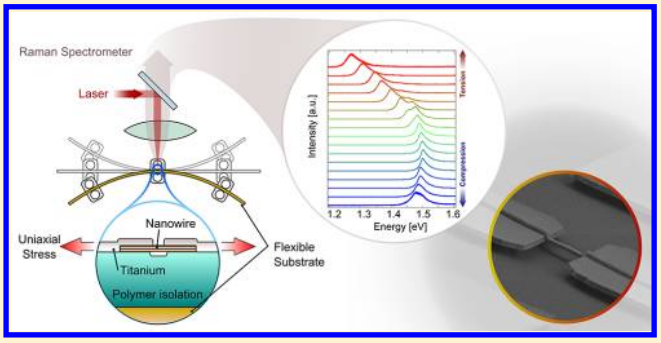

KEYWORDS: *Nanowire, GaAs, core−shell, uniaxial strain, photoluminescence, Raman, Poisson ratio, deformation potentials*

Strain engineering has proved to be a powerful strategy to enhance the performance of electronic as well as optoelectronic devices. In complementary metal−oxide−semiconductor technology, the significant increase in charge-carrier mobility gained by the application of strain has facilitated the continued performance increase during scaling, especially below the 90 nm node.[1] In optoelectronics, especially in quantum-well lasers, strain has been used to improve and tailor the device characteristics by shifting the bandgap and thus the spectrum to a wavelength that may not be achievable otherwise.[2−5] Furthermore, the density of states (DOS) was changed by strain to improve laser performance, increasing the gain and reducing the lasing threshold.[6] Recently it has been shown that strain in Ge can induce a direct bandgap transition and hence allows photoluminescence (PL) and electroluminescence to be achieved over a broad spectrum that covers several optical communication windows,[7−9] thus potentially enabling new integrated photonic applications.

Nanostructures and in particular nanowires benefit from increased yield strength and exotic mechanical properties as compared to their bulk counterparts.[10−12] Higher tensile stress levels can be applied elastically to nanostructures, making nanowires a very attractive system for large modifications of the energy band structure. Large shifts of the bandgap and increased emission intensity have been observed in core−shell nanowires of GaAs/GaInP[13] or GaAs/GaP,[14] in which, as in most device applications, strain is induced by epitaxially growing lattice-mismatched films or by depositing films with an intrinsic stress. However, the stress achievable with this method is limited by the material system selected and remains fixed once the device has been fabricated.

To investigate how different values of strain affect the electronic and optical properties of a device, it is desirable to apply stress mechanically and continuously vary its amount. This has been achieved using, for example, wafer-bending tests[15] or diamond anvil cells.[16] Whereas in the latter high stress levels can be achieved only in the compressive hydrostatic regime, in the former both tensile and compressive stress are possible, but the maximum stress range accessible is limited. For example, for typical Si wafer-bending experiments, only 200 MPa can be applied before the die breaks.[17]

Mechanical properties of semiconducting nanowires have been the object of intense investigations. Variations in the elastic modulus, accompanied by an alteration of the electrical transport properties, have been observed in silicon, germanium, and GaAs nanowires.[18−21] Very recently, also the optical properties of nanowires under strain have attracted interest. For example, strain has been applied to tune the bandgap of ZnO

Received: October 4, 2012
Revised: December 1, 2012

   dx.doi.org/10.1021/nl303694c | *Nano Lett.* XXXX, XXX, XXX−XXX

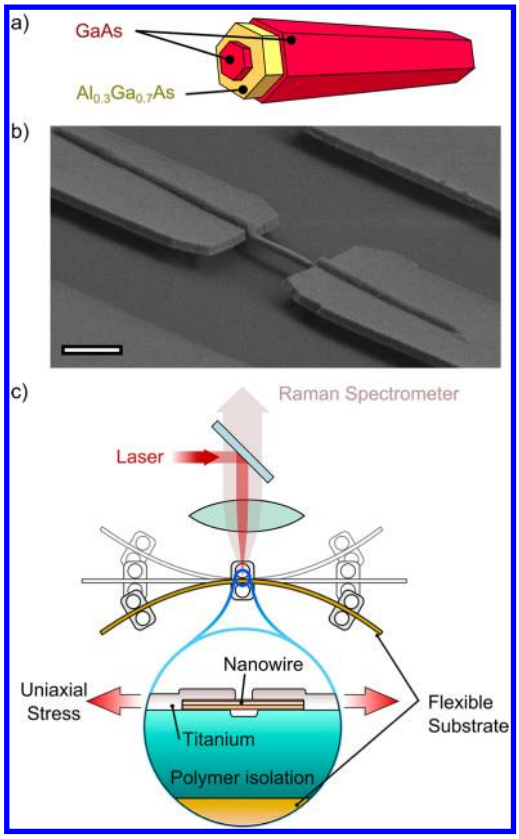

Figure 1. Application of stress to individual nanowires. (a) Schematic of a GaAs–$Al_{0.3}Ga_{0.7}As$–GaAs core–shell nanowire. (b) Scanning electron microscopy image of a freestanding nanowire clamped by Ti contacts to a flexible substrate. Scale bar is 1 μm. (c) Schematics of the bending mechanism used to apply stress to individual nanowires structures (shown in cross section). The nanowire is excited using a HeNe laser, and the PL and Raman signal are collected via an optical spectrometer.

nanowires[22] and to increase the conversion efficiency and intensity of ZnO nanowire-based LEDs.[23]

In this work, we investigate the influence of uniaxial tensile and compressive strain on the optical properties of GaAs nanowires as a model system for light-emitting materials. In particular, we show that uniaxial strain can be used to tune the emission spectrum of GaAs nanowires over a broad range in a continuous way. By straining the nanowire from −1.0 to 3.5% along its axis, a shift of the PL peak by more than 180 nm was achieved. Such a remarkable PL shift is possible because of the favorable mechanical properties of nanowires, which allow large strain to be applied elastically and reversibly.

We used GaAs–$Al_{0.3}Ga_{0.7}As$–GaAs core–shell nanowires, as schematically shown in Figure 1a. First the GaAs core was grown via vapor–liquid–solid technique at 360 °C in a metal–organic vapor-phase epitaxy system using gold as catalyst. Trimethylgallium (TMGa) and tertiarybutyl arsine (TBAs) sources were used with a TMGa molar flow of 10 μMol/min and a V/III ratio of 15 at a total pressure of 60 Torr. The $Al_{0.3}Ga_{0.7}As$ and GaAs shells were both grown at 650 °C with the addition of trimethyl aluminum at a flow rate of 10 μMol/min for the inner shell (6.66 μMol/min for TMGa and 3.33 μMol/min for TMAl). The GaAs nanowires are grown along the ⟨111⟩ direction with a diameter of 40 nm. The uniform 30-nm-thick $Al_{0.3}Ga_{0.7}As$ shell was grown to properly passivate the surface states on the GaAs core to enable stable PL.[24,25] Finally, the 3-nm-thick GaAs outer shell was grown to prevent oxidation of the $Al_{0.3}Ga_{0.7}As$ shell under ambient conditions. Strain effects induced by the AlGaAs shell should be negligible because of the almost perfect lattice match with the GaAs core (the relative difference in lattice constants is 0.04%). The wires have a uniform cross section and a length ranging between 7 and 8 μm. High-resolution transmission electron microscopy analysis of many wires reveals the crystal structure to be zincblende (ZB) and almost free of twin defects (on average less than one defect per micrometer).

To investigate how strain influences the optical properties of these wires, we fabricated doubly clamped nanowire structures on flexible stainless-steel substrates coated with a transparent polymer (shown in Figure 1b). Selected nanowires, transferred onto the substrate in the uniaxial strain direction, were fixed to the substrate surface by 180-nm-thick Ti metal clamps, fabricated using electron-beam lithography and lift-off. Finally, O_2 reactive-ion etching was performed to underetch and release the nanowire segment left uncovered by the metal clamps. The sample was then mounted into a three-point bending mechanism, as sketched in Figure 1c. Uniaxial compressive and tensile strain could be induced in the nanowire by bending the substrate in either concave or convex fashion, respectively, thus partially transferring the strain from the substrate surface to the nanowire via the metal and polymer supports. The strain induced was perfectly uniaxial because the increase in bending angle across the free-standing nanowire length (1 μm) is less than 10^{-6} degrees per percent of strain. The bending mechanism is mounted on a cryostat that allows temperature control in the range of 10–350 K under ultrahigh vacuum. Unless mentioned otherwise, PL and Raman spectra were measured as a function of the stress applied to the nanowires with the cryostat at a temperature of 100 K. In all experiments, a HeNe laser (λ = 632.8 nm) was focused by a 100× objective (numerical aperture = 0.8) onto a diffraction-limited spot of 0.7 μm (full-width half-maximum, FWHM) and used to excite the free-standing nanowire. The laser power was kept constant at 450 μW to minimize heating of the nanowire and to achieve a good signal-to-noise ratio. PL and Raman spectra were measured with a single-stage confocal Raman spectrometer (Horiba Scientific LabRam HR), equipped with a custom-made system consisting of motor-controlled rotatable achromatic half-wave plates and nanoparticle linear film polarizers to control the polarization in the excitation and the analytic path.

In Figure 2a, the PL spectrum of a nanowire at zero applied stress measured at a cryostat temperature of 100 K is shown. A single sharp peak, positioned at 1.487 eV with a FWHM of 30 meV, is observed. The PL peak position corresponds well with a nanowire temperature of 160 K, estimated both by comparing the peak value with the Varshni equation for bulk GaAs[26] and by fitting the PL spectrum with an inhomogeneously broadened peak described by a bulk-like joint density of states populated according to the Boltzmann distribution. We believe that the nanowire temperature is higher than the one of the cryostat because of laser-induced heating and restricted thermal coupling to the substrate. The relatively small FWHM of 30 meV and the high emission intensity, even at room temperature, are evidence of the small nonradiative defect density and the high quality of the wires studied here.[24,25] The Raman spectrum of the same nanowire measured at 100 K (Figure 2b) exhibits the characteristic peaks of the GaAs and $Al_{0.3}Ga_{0.7}As$ optical phonons. The GaAs transverse optical (TO) and longitudinal optical (LO) phonon peaks are located at 271.6

dx.doi.org/10.1021/nl303694c | *Nano Lett.* XXXX, XXX, XXX–XXX

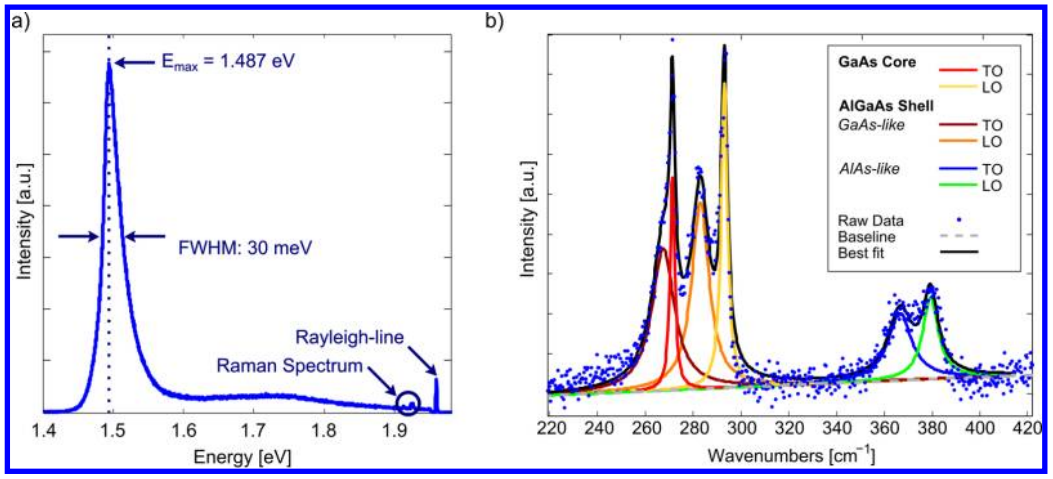

Figure 2. Optical spectrum of an individual nanowire at zero applied stress. (a) PL spectrum recorded at low temperature (cryostat temperature of 100 K) exhibiting a single peak at 1.487 eV, attributed to the GaAs core. A small luminescence background, originating from the nanowire shell and from the polymeric substrate, is visible in the range between 1.6 and 1.8 eV. The peaks at higher energies represent the Raman spectrum and the Rayleigh line (suppressed above 1.95 eV by the spectrometer's long-pass filter). (b) Raman spectrum measured (blue dots) for the same wire as in panel a and deconvolution of the optical phonon contributions (obtained by least-squares fitting). Listed in order from lowest to highest energy, the following phonon contributions are identified: GaAs-like TO from the $Al_{0.3}Ga_{0.7}As$ shell (brown) at 267.8 cm^{-1}; TO from the GaAs core (red) at 271.6 cm^{-1}; GaAs-like LO from the $Al_{0.3}Ga_{0.7}As$ shell (orange) at 283.2 cm^{-1}; LO from the GaAs core (yellow) at 293.1 cm^{-1}; AlAs-like TO from the $Al_{0.3}Ga_{0.7}As$ shell (blue) at 365.5 cm^{-1}; AlAs-like LO from the $Al_{0.3}Ga_{0.7}As$ shell (green) at 378.2 cm^{-1}. The black line represents the best fit.

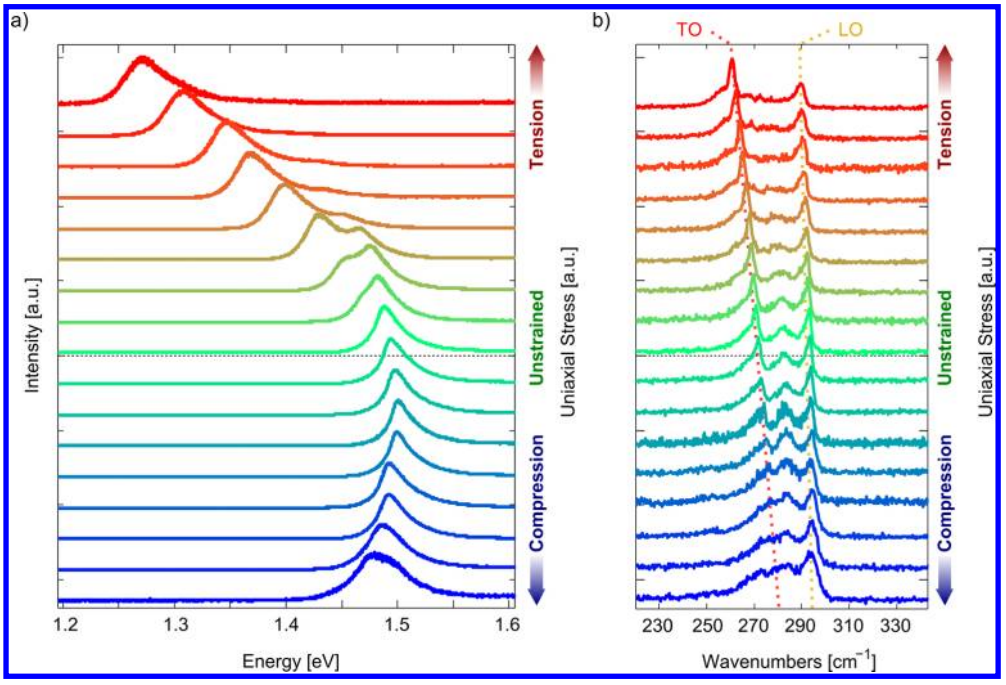

Figure 3. Effect of tensile and compressive stress on the optical properties of the core−shell GaAs−$Al_{0.3}Ga_{0.7}As$−GaAs nanowire. (a) PL spectra measured for different values of applied uniaxial stress. Under compression, the peak shifts weakly and nonlinearly with increasing stress, whereas under tension, a peak splitting is observed together with a strong red shift for the low-energy contribution. (b) Normalized Raman spectra of the GaAs-like phonons (230−330 cm^{-1}) for different values of uniaxial stress. All Raman peaks are observed to shift linearly with stress to higher wavenumbers under compression and to lower wavenumbers under tension. A guide to the eye is included for the peak position of the TO and LO of the GaAs core.

and 293.1 cm^{-1}, within few wavenumbers from the values of bulk.[27] Further peaks attributed to the AlGaAs shell are positioned at 267.8 (GaAs-like TO), 283.2 (GaAs-like LO), 365.5, and 378.2 cm^{-1} (AlAs-like TO and LO).[27] From the peak position of the AlGaAs LO phonons, we can estimate an Al concentration of (30 ± 1)% in the AlGaAs shell. The PL and Raman spectra could be measured reproducibly on all wires inspected, indicating the high quality of the wires grown.

The effect of the crystal deformation on the emission properties is presented in Figure 3a, in which the normalized PL spectra of an individual wire are plotted as a function of energy for different values of uniaxial stress. The spectrum at the dashed line corresponds to the signal of the unstrained wire. Under compression, the peak originally found around 1.48 eV shifts to slightly higher energies with increasing stress and exhibits a maximum of 1.50 eV. Increasing the stress further will

dx.doi.org/10.1021/nl303694c | *Nano Lett.* XXXX, XXX, XXX−XXX

broaden the spectrum and decrease the peak energy slightly. A much stronger peak shift toward lower energies is observed when tensile stress is applied. For moderate applied tension, a splitting of the PL peak into two components can be resolved. The component with the lowest energy experiences a strong red shift of up to 256 meV with increasing stress.

To understand the significantly asymmetric effect of strain, it is important to quantify how much strain is induced in the nanowire. For this, we analyze the Raman spectra in detail and use them to gauge the strain. The corresponding Raman spectra are plotted in Figure 3b as a function of wavenumber for different stress values. All Raman peaks are observed to shift linearly with applied uniaxial stress in the regime we investigated. Tensile stress decreases the energy of all phonons, whereas compressive stress causes their energies to increase. As we are interested in the strain effects of the nanowire core, we concentrate on the peak shift of the phonons assigned to the GaAs core: we find that the TO phonon experiences a stronger energy shift (15 cm^{-1}) than the LO peak (5 cm^{-1}). The observed stress effects on the PL and Raman spectra are fully reversible and reproducible for all nanowires in the regime tested.

To evaluate the axial strain applied to the wire from the Raman spectra, the predominant phonon contributions have to be identified. To this end, it is important to inspect the backscattering geometry used in our experiment, shown in the inset of Figure 4. In this configuration, the momentum of the phonons observed in the Raman spectra is, to first approximation, directed parallel to the incoming laser photon direction (i.e., the x-axis direction). Only one of the two TO phonons has an atomic displacement[28] along the direction of the nanowire axis (the z-axis). The atomic displacements of the remaining TO and LO lie instead in the nanowire cross-section plane, with the TO oriented along the y-axis and the LO along the x-axis. At zero applied stress, the two TO phonons are degenerate. However, when uniaxial strain is applied the resulting anisotropic deformation reduces the crystal symmetry and lifts the TO degeneracy. In particular, the TO phonon with atomic displacement along the nanowire axis (labeled TO_S after Cerdeira et al.[29,30]) is expected to experience a larger energy shift with strain than the other phonons (labeled TO_D and LO_D).

To identify which of the two TO phonons dominates the spectrum in Figure 3b, we can use the polarization dependence given by the Raman selection rules. Experimentally we can study two distinct configurations as shown in Figure 4. In both, the incoming laser light is polarized along the nanowire axis, that is, the z-axis, to maximize the interaction of light with the nanowire.[31] In the first scattering configuration, indicated[28] as $\bar{x}(z,y)x$, the light is detected orthogonal to the nanowires axis and hence only the TO_D should be visible. In the second scattering configuration, indicated as $\bar{x}(z,z)x$, we collect light polarized along the nanowire axis and hence expect only the TO_S to be visible. In Figure 4, the Raman spectra acquired at room temperature on a nanowire under high tensile stress are shown. The lower curve (green) has been measured with the first scattering configuration and both TO_S at 260 cm^{-1} and TO_D at 266 cm^{-1} can be observed. The TO_S phonon could not be completely suppressed in this configuration because of the finite angle of collection (53°).[32,33] The upper curve (blue) shows the spectrum acquired in the second configuration. The TO peak is located at the same energy as the contribution assigned to the TO_S phonon, whereas the TO_D contribution is

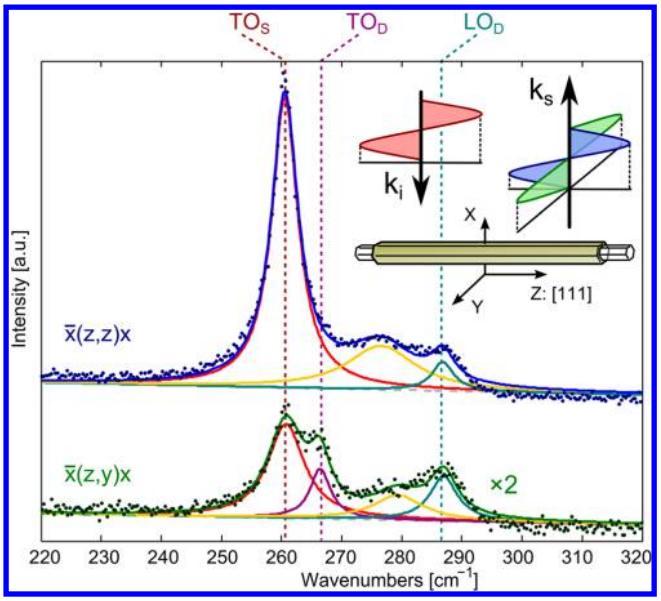

Figure 4. Room-temperature Raman spectra of a nanowire under high tensile stress in two distinct scattering configurations, depicted in the inset. The laser light polarization is oriented along the nanowire axis. In the first scattering configuration ($\bar{x}(z,y)x$, in green), the scattered light with polarization orthogonal to the nanowire axis is selected and measured. The TO phonon with the atomic displacement directed along the nanowire axis (TO_S, plotted in red) undergoes the highest shift toward low energies with an energy of 260.5 cm^{-1}. The energy of the remaining two phonons of the GaAs core can also be identified (LO_D, plotted in turquoise, and TO_D, plotted in purple): these two phonons have an atomic displacement lying in the nanowire cross-sectional plane, and their energy is 266.3 and 286.4 cm^{-1}, respectively. In the second configuration ($\bar{x}(z,z)x$, in blue), the Raman spectrum is measured by collecting scattered light with polarization parallel to the nanowire, and only the TO_S and LO_D phonons are visible. The peaks observed around 275 and 280 cm^{-1} (plotted in yellow) are attributed to the GaAs-like LO phonon of the $Al_{0.3}Ga_{0.7}As$ shell.

completely suppressed. The agreement between the measured Raman spectral intensities and the expected polarization dependencies confirms the assignment of TO_D and TO_S. We can also conclude that TO_S and LO_D provide the dominating phonon contributions in the Raman spectra shown in Figure 3b.

To estimate the axial strain in the wire, we can use the linear relation between the relative energy shift of the TO_S and LO_D phonons[29] and the axial strain ε_{zz} in the nanowire, expressed in the following set of equations:

$$\begin{cases} \dfrac{\Delta\omega_{TO_S}}{\omega_{TO_S}} = [-3\gamma_T H + r'_T(1-H)]\varepsilon_{zz} \\ \dfrac{\Delta\omega_{LO_D}}{\omega_{LO_D}} = \left[-3\gamma_L H - \dfrac{1}{2}r'_L(1-H)\right]\varepsilon_{zz} \end{cases}$$
$$\text{with } H = \frac{1-2\nu}{3} \qquad (1)$$

where $\gamma_T = 1.35$ and $\gamma_L = 1.07$ are the hydrostatic phonon deformation potentials (also known as Grüneisen parameters), $r'_T = -0.88$ and $r'_L = -0.53$ are the shear deformation potentials for the GaAs TO and LO phonons,[30] and ν is the nanowire Poisson ratio for the ⟨111⟩ direction. Note that H represents the portion of nanowire elongation caused by the

dx.doi.org/10.1021/nl303694c | Nano Lett. XXXX, XXX, XXX−XXX

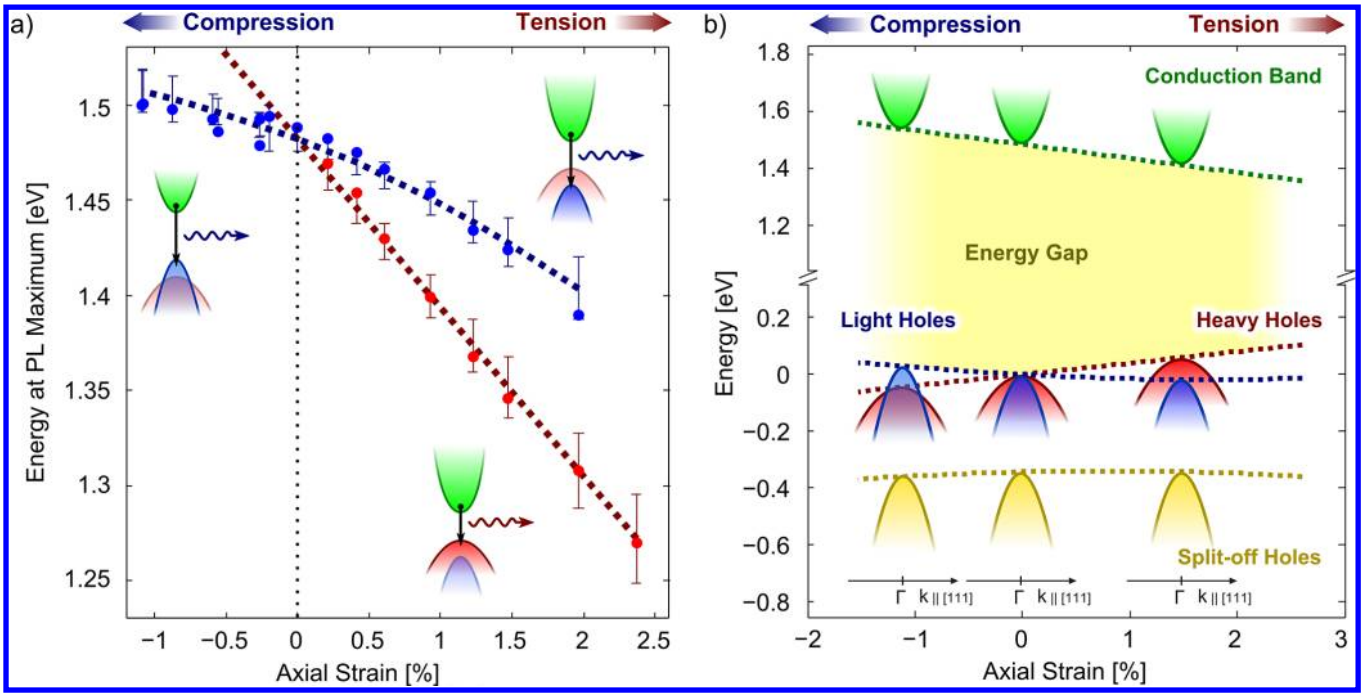

Figure 5. PL peak energy and simulated energy shifts of the conduction and valence band edges as a function of the quantified axial strain applied to the core−shell GaAs−$Al_{0.3}Ga_{0.7}As$−GaAs nanowire. (a) PL peak positions of the nanowire vs strain. Red data points are attributed to the recombination from the conduction band (shown in green) to the heavy-hole band (shown in red), whereas blue data points describe transitions from the conduction band to the light-hole band (shown in blue). The dotted lines result from a fit of the data points with an 8-band k·p model using bulk deformation potentials and the extracted nanowire axial strain, Poisson ratio, and bandgap in unstrained conditions. The error bars show the uncertainty in the estimation of the PL shift due to the uncertainty in the Poisson ratio (0.16 ± 0.04), in the axial strain (more than 0.14% of strain, see Supporting Information) and the energy bandgap (1.482 eV ± 5 meV). (b) Expected shift of the band edges according to an 8-band k·p model. Heavy-hole band (red) and conduction band (green) edges shift linearly in energy with opposite slope. The light-hole band (blue) energy follows a quadratic dependence on uniaxial stress because of strain mediated spin−orbit interaction with the split-off band (yellow). The small bandgap variation under compression is due to a similar shift of the heavy-hole band and the conduction band in this stress regime. The substantial red shift observed under tension is related to the change in the symmetry character of the highest energy valence band from light-hole to heavy-hole type.

isotropic component of the ZB unit-cell deformation, whereas $(1 - H)$ is the remaining fraction of elongation due to the shear deformation of the ZB unit cell.

To extract the axial strain of the nanowire, we assume that the bulk GaAs phonon deformation potentials well describe the shifts we observe in our wire. This assumption is justified by independent measurements performed by Zardo et al.[34,35] in similar wires under hydrostatic strain. In these measurements, a value of the hydrostatic deformation potential close to that of bulk GaAs (within 30%) has been extracted. Under this assumption, we can estimate the axial strain in the nanowire and infer the Poisson ratio in the ⟨111⟩ direction. Interestingly, we notice that the Poisson ratio estimated for the nanowire (0.16) is smaller than that measured in bulk GaAs (0.186) for the same stress direction.

Using the axial strain estimation, we proceed to analyze the PL spectra of Figure 3 quantitatively. In Figure 5a, the PL peak energies are plotted as a function of the axial strain induced in the nanowire. The analysis shows that the nanowire experiences a compressive strain of up to −1.0% and a tensile strain of up to 2.4% (the respective measurement uncertainties are reported in the Supporting Information). These values are within the expected limits imposed by buckling[36] and plastic deformation. In compression, the peak wavelength varies only weakly, whereas in tension a much stronger dependence together with a peak splitting can be observed. Both peaks red-shift significantly under tension, by 85 meV/% for the lower energy peak and by approximately 56 meV/% for the higher energy one.

The shifts of the PL peaks vs axial strain are directly related to the energy shifts of the conduction and valence band edges, which can be described using an 8-band k·p model that includes the Pikus−Bir strain Hamiltonian.[37,38] The expected energy-level shifts are plotted in Figure 5b. As soon as uniaxial stress is applied to the nanowire, the valence band degeneracy between light-hole and heavy-hole is lifted because of the symmetry-breaking shear deformation of the ZB unit cell.[44,45] On the one hand, the conduction band will shift because of the volume-changing isotropic deformation component of the strain. Interestingly, the conduction band edge (represented in green) and the heavy-hole band (represented in red) shift linearly with strain with opposite slopes, whereas the light-hole band (represented in blue) follows a quadratic behavior because of the strain−mediated spin−orbit interaction and mixing with the split-off band (represented in yellow).

The selection rules identify which optical transitions are allowed for a specific light polarization: recombination into the heavy-hole can generate light only with polarization perpendicular to the strain axis,[39] whereas light emitted from the recombination into the light-hole states can have polarization either parallel or perpendicular to the stress axis (polarization-resolved PL measurements are shown in the Supporting Information). Moreover, the nanowire geometry influences the emission of the luminescence into the environment: because of

dx.doi.org/10.1021/nl303694c | Nano Lett. XXXX, XXX, XXX−XXX

the high dielectric mismatch between the nanowire and the environment, the light emitted perpendicular to the nanowire axis will couple out with an efficiency lower than one order of magnitude compared to the light polarized parallel to the nanowire axis.[40,41] For our specific case, the luminescence originating from the heavy-hole recombination will therefore be strongly suppressed, whereas the one coming from the light-hole will be affected less strongly. Dielectric mismatch and selection rules fully describe which recombination processes can be observed in the PL spectra.

Under tension, both the light-hole band and the conduction band shift down in energy, whereas the heavy-hole band shifts up. In this stress regime, the band gap is defined by the heavy-hole band and the conduction band. These bands shift toward each other and generate the large red shift. For high values of stress, only the recombination from heavy-hole states can be observed, although affected by the dielectric mismatch effects. For small values of stress that induce a valence-band splitting smaller than a few kT, both heavy- and light-hole states can be populated and the respective recombination processes observed as a peak splitting. The light-hole band will be populated with fewer holes, but its recombination will not suffer from dielectric mismatch effects. Conversely, the higher population of the heavy-hole is balanced by the poorer coupling of its luminescence due to dielectric mismatch.

Under compression, both the light-hole band edge and the conduction band edge shift toward higher energies, whereas the heavy-hole band shifts down in energy.[42] The light-hole states are therefore energetically favored and populated with highest density, while the corresponding luminescence is efficiently coupled to the environment. Heavy-hole states will instead be poorly populated and the corresponding luminescence attenuated because of dielectric mismatch effects. As a consequence only the PL peak due to light-hole recombination can be observed. Note that the conduction band and the light-hole band undergo similar shifts under strain and, consequently, the energy gap does not vary substantially under compression.

The variation of the energy difference between the conduction band and the two valence bands as a function of the axial strain, ε_{zz}, can be approximately expressed[37] with the following set of relations:

$$\begin{cases} \Delta E_{\mathrm{CB-LH}} = \left[3aH - \dfrac{\sqrt{3}}{2}d(1-H)\right]\varepsilon_{zz} \\ \qquad\qquad - \dfrac{3d^2(1-H)}{2\Delta_0}{\varepsilon_{zz}}^2 \\ \Delta E_{\mathrm{CB-HH}} = \left[3aH + \dfrac{\sqrt{3}}{2}d(1-H)\right]\varepsilon_{zz} \end{cases} \quad (2)$$

where $\Delta E_{\mathrm{CB-HH}}$ is the energy of the transitions into the heavy-hole band, $\Delta E_{\mathrm{CB-LH}}$ is the energy of the transitions into the light-hole band, Δ_0 is the spin−orbit splitting, and a and d are, respectively, the hydrostatic and shear optical deformation potentials. The factor H has been introduced in equation 1 and is linearly dependent on the Poisson ratio. Using this model as well as the axial strain and Poisson ratio obtained from the Raman spectra, we can extract the hydrostatic deformation potential $a = -8.6 \pm 0.7$ eV and the shear deformation potential $d = -5.2 \pm 0.7$ eV. Both values are very similar to those observed in bulk GaAs, and provide the final confirmation of the integrity of our assumptions and of the axial strain estimation.[42,43] We also note that the finite nanowire size plays an important role in determining the PL shifts because of its effect on the mechanical properties. As the Poisson ratio decreases, the factor H increases together with the hydrostatic deformation component of the nanowire elongation. As a consequence, the hydrostatic deformation potential a (which is larger than the shear deformation potential d) will increase its influence in the weighted sums in equation 2, resulting in an amplification of the PL shift with strain. Finite-size effects can therefore be used to tune the mechanical properties of the nanowire and to boost strain effects.

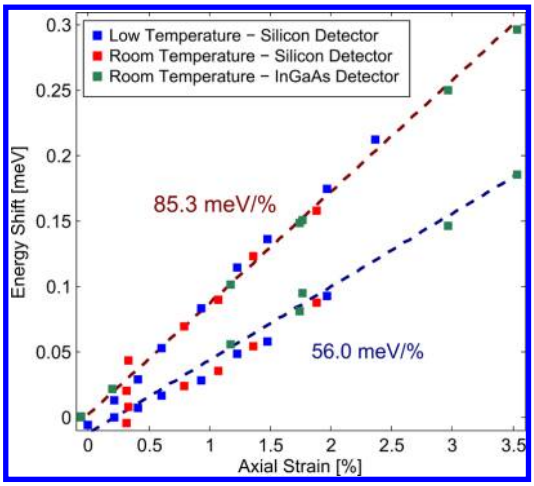

Figure 6. Energy shift for the light-hole and heavy-hole band transitions vs tensile uniaxial strain in the nanowire. The blue squares are extracted from the low-temperature data shown in Figure 3. The red squares result from measurements performed on the same wire at room temperature. The green squares are extracted from room-temperature measurements performed on a different wire with an InGaAs detector, to expand the spectrometer spectral range of sensitivity of the silicon detector beyond 1.2 eV. The energy of the transition into the heavy-hole band (dashed red line) is observed to shift with 85.3 meV/% of tensile strain, whereas the energy of the transition into the light-hole band (dashed blue line) shifts approximately with 56.0 meV/%. All three data sets follow the same trend, suggesting that deformation potentials and mechanical properties exhibit no substantial temperature dependence between 100 K and room temperature. The maximum PL shift observed is of 296 meV, corresponding to 3.5% tensile strain.

Furthermore, we have also investigated the effect of strain at room temperature. In Figure 6, we show the energy shift in PL measured at different temperatures in the tensile regime. The blue squares are extracted from the low-temperature data already presented, whereas the red squares are derived from measurements of the same wire at room temperature. Both data sets follow the same trend, suggesting that deformation potentials and elastic constants exhibit no substantial temperature dependence between 160 K and room-temperature.

To measure the effect of higher strain, we used an InGaAs detector to expand the spectral range of sensitivity beyond 1.2 eV (the limit of the silicon detector). The corresponding shift in PL peak energy, measured on a different wire, is shown as green squares in Figure 6. We were able to induce a noticeably high strain of 3.5% and achieve a maximum red shift of 296 meV. To our knowledge, this is the highest tensile strain ever reported on a working GaAs nanostructure. Upon further

dx.doi.org/10.1021/nl303694c | Nano Lett. XXXX, XXX, XXX−XXX

stretching, the PL shifted back to its relaxed position. This could be related to a rupture of the wire or to the slippage of the nanowire under the metal clamps.

In summary, we investigated the effect of strain on the photoluminescence and Raman spectra of GaAs/$Al_{0.3}Ga_{0.7}As$/GaAs core/shell nanowires. Uniaxial stress was applied mechanically to the nanowire in a continuous and reversible way, both in compression and tension. Upon application of tension, we observed a highly asymmetric shift of the PL and a remarkable decrease of the band gap of 296 meV at 3.5% of strain. Fingerprints of symmetry breaking due to the anisotropic nature of the nanowire deformation were found in the PL and in the Raman spectra, in which polarization-dependent measurements allowed us to univocally identify the distinct phonon contributions.

Because of its linear relation with stress, the energy shift of the Raman peaks was used to determine the axial strain induced in the nanowire and to obtain information about the Poisson ratio in the ⟨111⟩ direction. The significant change in the electronic bandstructure is explained using an 8-band k·p model, and deformation potentials consistent with those of the bulk were extracted.

Given the high value for the yield strength and the high elongation that can be elastically induced, GaAs semiconducting nanowires are the ideal platform to realize optoelectronic devices that leverage strain effects to tune the optical properties over a broad wavelength range.

■ ASSOCIATED CONTENT

Supporting Information

Additonal information and figures. This material is available free of charge via the Internet at http://pubs.acs.org.

■ AUTHOR INFORMATION

Corresponding Author

*E-mail: gio@zurich.ibm.com.

Present Address

[†]QuNano AB, Scheelevägen 17, Ideon Science Park, 22370 Lund, Sweden.

Notes

The authors declare no competing financial interest.

■ ACKNOWLEDGMENTS

The authors gratefully acknowledge E. Lörtscher, who designed and established the tool to perform the low-temperature strain measurements, and V. Schmidt, C. Tuma, P. Khomyakov, H. Weman, C. Schönenberger, G. Isella, A. Schenk, M. Cardona, and W. Riess for fruitful discussions. We further acknowledge H. Schmid, T. Topuria, P. Rice, C. Rettner, U. Drechsler, M. Tschudy, and S. Baier for technical support. The research leading to these results has received funding from the European Union Seventh Framework Program (FP7/2007-2013) FUNMOLS under Grant Agreement [212942] and Steeper under Grant Agreement [257267].

■ REFERENCES

(1) Chan, V.; Rengarajan, R.; Rovedo, N.; Hook, T.; Nguyen, P.; Nowak, E.; Lea, D.; Chakravarti, A.; Ku, V.; Yang, S.; Steegen, A.; Baiocco, C.; Shafer, P.; Wann, C. *Electron Devices Meeting, 2003. IEDM '03 Technical Digest. IEEE International* **2003**, 3.8.1−3.8.4.

(2) Kikuchi, A.; Kishino, K.; Kaneko, Y. *Jpn. J. Appl. Phys.* **1991**, *30*, 3865−3872.

(3) Hamada, H.; Tominaga, K.; Shono, M.; Honda, S.; Yodoshi, K.; Yamaguchi, T. *Electron. Lett.* **1992**, *28*, 1834.

(4) Bour, D. P.; Treat, D. W.; Beernink, K. J.; Krusor, B. S.; Geels, R. S.; Welch, D. F. *IEEE Photonics Technol. Letters* **1994**, *6*, 128−131.

(5) Tanaka, S.; Lundstrom, M. S. *Solid-State Electron.* **1994**, *37*, 401−410.

(6) Silver, M.; O'Reilly, E. P. *IEEE J. Quantum Electron.* **1994**, *30*, 547−553.

(7) Huo, Y.; Lin, H.; Chen, R.; Makarova, M.; Rong, Y.; Li, M.; Kamins, T. I.; Vuckovic, J.; Harris, J. S. *Appl. Phys. Lett.* **2011**, *98*, 011111.

(8) Saito, S.; Oda, K.; Takahama, T.; Tani, K.; Mine, T. *Appl. Phys. Lett.* **2011**, *99*, 241105.

(9) Sun, X.; Liu, J.; Kimerling, L. C.; Michel, J. *Appl. Phys. Lett.* **2009**, *95*, 011911.

(10) Gordon, M. J.; Baron, T.; Dhalluin, F.; Gentile, P.; Ferret, P. *Nano Lett.* **2009**, *9*, 525−9.

(11) Han, X. D.; Zheng, K.; Zhang, Y. F.; Zhang, X. N.; Zhang, Z.; Wang, Z. L. *Adv. Mater.* **2007**, *19*, 2112−2118.

(12) Sohn, Y.-S.; Park, J.; Yoon, G.; Song, J.; Jee, S.-W.; Lee, J.-H.; Na, S.; Kwon, T.; Eom, K. *Nanoscale Res. Lett.* **2009**, *5*, 211−216.

(13) Sköld, N.; Karlsson, L. S.; Larsson, M. W.; Pistol, M.-E.; Seifert, W.; Trägårdh, J.; Samuelson, L. *Nano Lett.* **2005**, *5*, 1943−7.

(14) Montazeri, M.; Fickenscher, M.; Smith, L. M.; Jackson, H. E.; Yarrison-Rice, J.; Kang, J. H.; Gao, Q.; Tan, H. H.; Jagadish, C.; Guo, Y.; Zou, J.; Pistol, M.-E.; Pryor, C. E. *Nano Lett.* **2010**, *10*, 880−6.

(15) Thompson, S. E.; Suthram, S.; Sun, Y.; Sun, G.; Parthasarathy, S.; Chu, M.; Nishida, T. *Electron Devices Meeting, 2006. IEDM '06 Technical Digest. IEEE International* **2006**, 1−4.

(16) Goñi, A. R.; Syassen, K. In *High Pressure in Semiconductor Physics*; Academic Press: London, 1998; Vol. *1*, pp 248−410.

(17) Choi, Y. S.; Numata, T.; Nishida, T.; Harris, R.; Thompson, S. E. *J. Appl. Phys.* **2008**, *103*, 064510.

(18) Smith, D.; Holmberg, V. C.; Korgel, B. A. *ACS Nano* **2010**, *4*, 2356−62.

(19) Wang, Y.-B.; Wang, L.-F.; Joyce, H. J.; Gao, Q.; Liao, X.-Z.; Mai, Y.-W.; Tan, H. H.; Zou, J.; Ringer, S. P.; Gao, H.-J.; Jagadish, C. *Adv. Mater.* **2011**, *23*, 1356−60.

(20) He, R.; Yang, P. *Nat. Nanotechnol.* **2006**, *1*, 42−6.

(21) Lugstein, A.; Steinmair, M.; Steiger, A.; Kosina, H.; Bertagnolli, E. *Nano Lett.* **2010**, *10*, 3204−8.

(22) Wei, B.; Zheng, K.; Ji, Y.; Zhang, Y.; Zhang, Z.; Han, X. *Nano Lett.* **2012**, *12*, 4595−9.

(23) Yang, Q.; Wang, W.; Xu, S.; Wang, Z. L. *Nano Lett.* **2011**, *11*, 4012−7.

(24) Wolford, D. J. *J. Vac. Sci. Technol., B: Microelectron. Nanometer Struct.* **1991**, *9*, 2369.

(25) Titova, L. V.; Hoang, T. B.; Jackson, H. E.; Smith, L. M.; Yarrison-Rice, J. M.; Kim, Y.; Joyce, H. J.; Tan, H. H.; Jagadish, C. *Appl. Phys. Lett.* **2006**, *89*, 173126.

(26) Adachi, S. *GaAs and Related Materials: Bulk Semiconducting and Superlattice Properties*; World Scientific: New York, 1994; p 675.

(27) Adachi, S. *J. Appl. Phys.* **1985**, *58*, R1−R29.

(28) Cardona, M.; Yu, P. Y. *Fundamentals of Semiconductors: Physics and Materials Properties*; Springer: New York, 2010; p 775.

(29) Cerdeira, F.; Buchenauer, C.; Pollak, F. H.; Cardona, M. *Phys. Rev. B* **1972**, *5*, 580.

(30) Wickboldt, P.; Anastassakis, E.; Sauer, R.; Cardona, M. *Phys. Rev. B* **1987**, *35*, 1362.

(31) Chen, G.; Wu, J.; Lu, Q.; Gutierrez, H. R.; Xiong, Q.; Pellen, M. E.; Petko, J. S.; Werner, D. H.; Eklund, P. C. *Nano Lett.* **2008**, *8*, 1341−6.

(32) Bonera, E.; Fanciulli, M.; Batchelder, D. N. *J. Appl. Phys.* **2003**, *94*, 2729.

(33) Ossikovski, R.; Nguyen, Q.; Picardi, G.; Schreiber, J. *J. Appl. Phys.* **2008**, *103*, 093525.

(34) Zardo, I. In *Selected Topics of Semiconductor Physics and Technology*; Verein zur Förderung des Walter Schottky Instituts der Technischen Universität München: München, 2010; Vol. *122*, p 184.

(35) Zardo, I.; Yazji, S.; Marini, C.; Uccelli, E.; Fontcuberta i Morral, A.; Abstreiter, G.; Postorino, P. *ACS Nano* **2012**, *6*, 3284−91.
(36) Fang, W.; Wickert, J. A. *J. Micromechan. Microeng.* **1994**, *4*, 116−122.
(37) Bir, G. L.; Pikus, G. E. *Symmetry and Strain-Induced Effects in Semiconductors*; Wiley: New York, 1974; p 484.
(38) Gershoni, D.; Henry, C. H.; Baraff, G. A. *IEEE J. Quantum Electron.* **1993**, *29*, 2433−2450.
(39) Pollak, F.; Cardona, M.; Shaklee, K. *Phys. Rev. Lett.* **1966**, *16*, 942−944.
(40) Ruda, H.; Shik, A. *Phys. Rev. B* **2005**, *72*, 1−11.
(41) Wang, J.; Gudiksen, M. S.; Duan, X.; Cui, Y.; Lieber, C. M. *Science (N. Y.)* **2001**, *293*, 1455−7.
(42) Chandrasekhar, M.; Pollak, F. *Phys. Rev. B* **1977**, *15*, 2127−2144.
(43) Van de Walle, C. *Phys. Rev. B* **1989**, *39*, 1871−1883.
(44) Pollak, F. F. H.; Cardona, M. *Phys. Rev.* **1968**, *172*, 816−837.
(45) We follow an established notation used in ref 44 that indicates, respectively, with heavy, light and split-off hole the states $|3/2, \pm 3/2\rangle$, $|3/2, \pm 1/2\rangle$ and $|1/2, \pm 1/2\rangle$, where the first quantum number is the total angular momentum, while the second one is its projection along the uniaxial strain direction.

dx.doi.org/10.1021/nl303694c | *Nano Lett.* XXXX, XXX, XXX−XXX